ARTICLE

Thermo-Mechanical Modeling of High-Strength Concrete Column Subjected to Moderate Case Heating Scenario in a Fire

Tarek Eltalhi[1]   Awad S. Bodalal[1]   Farag M. Shuaeib[1]   Vail Karakale[2*]

1. Mechanical Engineering Department, Faculty of Engineering, University of Benghazi, Benghazi, 00218, Libya
2. Civil Engineering Department, Faculty of Engineering and Natural Sciences, Istanbul Medeniyet University, Istanbul, 90212, Turkey

ABSTRACT

This paper presents a numerically developed computer model to simulate the thermal behavior and evaluate the mechanical performance of a fixed end loaded loaded High Strength Concrete Column (HSCC), subjected to Moderate Case Heating Scenario (MCHS), in a hydrocarbon fire. The temperature distribution within the mid-height cross-sectional area of the column was obtained to determine the thermal and mechanical responses as a function of temperature. The governing two-dimensional transient heat transfer partial differential equation (PDE), was converted into a set of ordinary algebraic equations, subsequently, integrated numerically by using the explicit finite difference method, (FDM). A computer program, Visual Basic for Applications (VBA), was then developed to solve the set of ordinary algebraic equations by implementing the boundary as well as initial conditions. The predictions of the model were validated against experimental data from previous studies. The general behavior of the model as well as the effect of the key model parameters were investigated at length in the review. Finally, the reduction in the column's compression strength and the modulus of elasticity was estimated using correlations from existing literature. And the HSCC failure load under fire conditions was predicted using the Rankine formula. The results showed that the model predictions of the temperature distribution within the concrete column are in good agreement with the experimental data. Furthermore, the increase in temperature of the reinforced concrete column, (RCC), due to fire resulted in a significant reduction in the column compression strength and considerably accelerates the column fire failure load.

1. Introduction

Naturally or intentionally, fire is a catastrophic disaster. When it is set, invariably a vast number of losses in both property and lives are expected. As an eyewitness, we have seen huge damage in buildings as a result of

*Corresponding Author:
Vail Karakale,
Civil Engineering Department, Faculty of Engineering and Natural Sciences, Istanbul Medeniyet University, Istanbul, Turkey;
Email: vail.karakale@medeniyet.edu.tr

the progression use of fire weapons during the Libyan civil war in 2011. On the other hand, the efforts of developing simulation models of fire effects on building's structural members will never stop saving people's lives and their properties.

When a building catches fire, the structural integrity and stability are dependent on the column's ability to resist failure at elevated temperatures, which is the first and last line of defense to maintain the column's strength. As a primary load-bearing member, the column is designed to withstand axial centric and/or eccentric loads of any structure. In other words, it carries the whole building's live and dead loads.

According to the related international standard codes, the fire resistance of any structural member is obtained experimentally. This is an expensive and time-consuming procedure and the utility of published experimental test data in a practical engineering design exercise is questionable. Although experimental studies are decisive, and the outcome is limited to the number of measurements taken during the test, experimental data can be used in the calibration and validity of the mathematical and numerical models, as mentioned in many studies [1-6].

While numerical simulation models generate much more useful interpretable data, there is a limit to which experimental tests can be conducted. Recently, emphasis is placed on mathematical simulation models to replace the existing experimental fire rating-based design methods with performance-based design procedures. Generally, concrete structural exhibits good performance under normal situations. However, results from several studies have shown that there are well-defined differences between the properties of high-strength concrete and normal-strength concrete during a fire since the former is much more durable and stronger than the latter. Furthermore, concerns have been developed regarding the reduction in strength of high-strength concrete when subjected to elevated temperature [7-13].

The main objective of this study is to develop a 2D numerical simulation basic computer model to predict the thermal behavior, to evaluate the mechanical performance of preloaded HSCC, and to set the failure criteria of the such column in a standard fire. The model development will be conducted by following the rule of elimination of some variables and parameters, and refining the code by neglecting non-significant parameters, assuming values for other factors, and using correlations and expressions from previous related studies to predict temperature distribution and strength profiles within the selected quarter cross-section area of the subjected HSCC.

1.1 Behavior of HSC Exposed to Fire

The fire-resistance rating of a concrete structural member is a function of applied load intensity and centricity, member type (e.g., column or beam or wall), member dimensions and boundary end conditions, incident heat flux from the fire on the member or assembly, type of construction materials (e.g., concrete, steel & wood) and finally, the effect of temperature rise within structural member on relevant properties of the member. The concrete is classified as Normal Strength Concrete (NSC), with a compressive strength of < 70 MPa, and High Strength Concrete (HSC) with a compressive strength of$\geq$ 70 MPa [14-17].

The use of HSC is widely increasing recently especially in High-rise buildings, offshore structures, and bridges because it has higher strength and improved durability compared to NSC, but in the fire incident, NSC performs better than HSC due to its low permeability reduces the effect of spalling in fire [17], as shown in Figures 1a and 1b.

a

b

Figure 1. a) NSCC in a fire exposure test; b) HSCC in a fire exposure test

Data from the experimental research that was carried out at specialized laboratories, as well as some worldwide organizations show that concentrically loaded and short

columns failed in pure compression while eccentrically loaded and long columns failed in combined flexure/compression mode due to buckling spalling [2,11-13]. Figures 2a and 2b for example show the effect of one of those factors namely the effect of the lateral reinforcement configuration on the spalling behavior in HSC Columns after the fire resistance test [17].

a

b

Figure 2. a) Conventional tie configuration; b) Modified tie configuration

1.2 The Effect of High Temperature on Steel Reinforced Concrete Structural Member

The fire performance of any structural member depends on the thermal and mechanical properties of the materials from which the building component is made. The critical temperature of fully-loaded structural member building materials such as steel and concrete is defined as the temperature at which the integrity of the member lost 50% of its original yield strength at 20 °C and becomes questionable. The building code requirements for structural fire protection are based on tests conducted following ASTM E-119. In these tests, the performance criteria for building assemblies, such as columns, is the loading bearing capacity, when these assemblies are exposed to heating conditions the mechanical properties that affect the fire performance of the structural members such as Compression Strength, Modulus of elasticity, Coefficient of thermal expansion, and Creep [4,18].

In the case of slender columns, the susceptibility for buckling increases with a decrease in the modulus of elasticity, and the concrete modulus of elasticity decreases rapidly with the rise of temperature. If steel reinforcement attains a temperature of 550 °C the modulus of elasticity is reduced to approximately half of the value at ambient and the concrete strength decrease is minimal up to about 300 °C, above these temperatures, the concrete strength loss is significant [12].

Steel-reinforced concrete columns are designed to withstand the applied load, although concrete will carry more load than steel, both will share the load in normal conditions [3]. When a column made of two different materials is subjected to fire under a given axial load at a certain temperature, one of those materials will carry the total load because of the thermal expansion differences, as there is no relative movement between concrete and steel in the reinforced concrete unit, elongation or contraction of both concrete and steel will be the same, equally strained before failure occurrence [18].

2. Materials and Methods

The thermal modeling that is used in this paper is based on the ASTM E-119 standard fire curve as shown in Figure 3 which describes the hydrocarbon fire development [2,17,19].
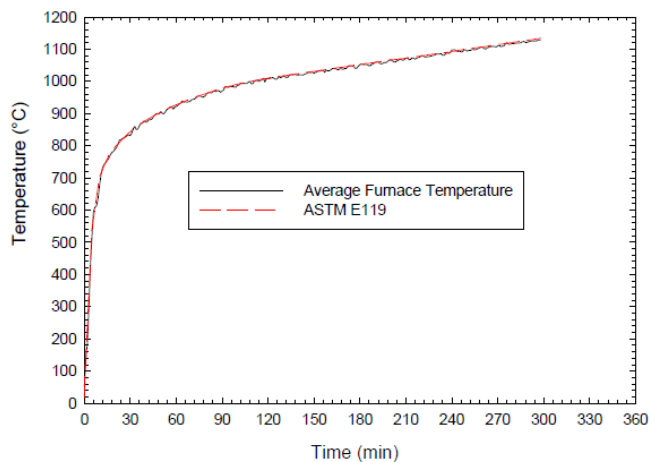
Figure 3. ASTM E-119 Standard temperature VS time

$$T(t) = T_0 + 750 \times \left(1 - e^{-3.79533 \sqrt{t}}\right) + 170.4 \times \sqrt{t} \quad (1)$$

where, t = time in hours, and T_0 = 20 °C, initial temperature used as boundary condition in both x and y directions.

2.1 Model Development

The physical description and cross-sectional configuration of the subjected HSCC which is surrounded by air with time-changing temperature according to E-119 are shown in Figures 4a and 4b.
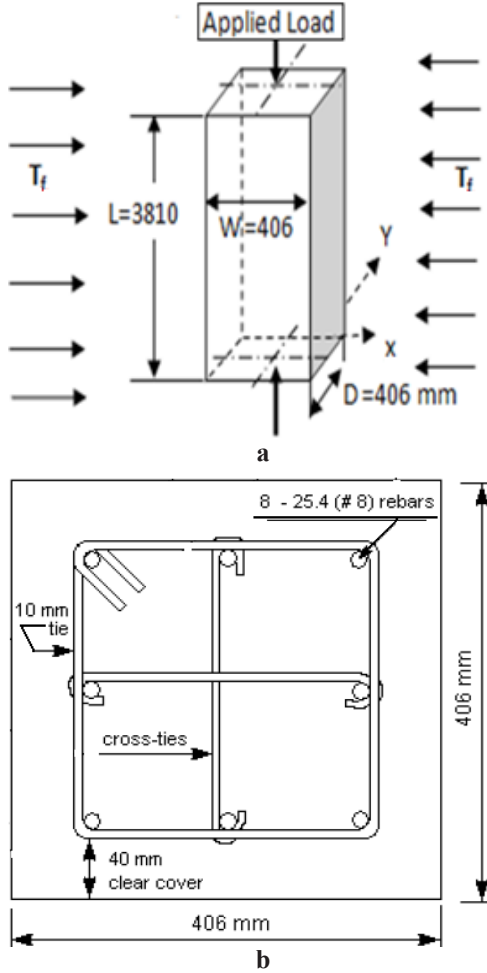
Figure 4. a) Physical description of the model; b) HSCC cross-sectional configuration

2.2 Equations and Key Assumptions

Basically, the heart of the model is the variable thermal boundary conditioned with the famous two-dimensional transient conduction heat transfer equation with constant thermal properties (Equation 1):

$$k \frac{\partial}{\partial x}\left[\frac{\partial T}{\partial x}\right] + k \frac{\partial}{\partial y}\left[\frac{\partial T}{\partial y}\right] + q = pc \frac{\partial T}{\partial t} \tag{2}$$

Divide both sides by k, neglecting heat generation inside the column $q = 0$, and replace $[k / (\rho c_p)]$ with thermal diffusivity (α), we get:

$$\frac{\partial^2 T}{\partial x^2} + \frac{\partial^2 T}{\partial y^2} = \frac{1}{\alpha} \frac{\partial T}{\partial t} \tag{3}$$

Then the central finite difference expression is used to approximate the partial differential second-order terms. Hence, a set of first-order Ordinary Differential Equations (ODE's) resulted.

2.3 Computation Domains and Solution Techniques

The first step in the formulation is to subdivide the x and y directions into equally spaced nodes. For the sake of numerical stability, the computational domain is divided into (W/2 = D/2 = 203 nodes) in each direction. To implement the boundary conditions the fire-exposed surfaces and symmetry lines nodes are formulated differently from the rest of the interior nodes.

Finally, the resulting set of (ODE's) is solved by using the explicit finite difference method and the 2-D transient temperature distributions within the concrete column is founded.

The two-dimensional transient conduction heat transfer configuration for the interior nodes according to FD numerical method procedure is shown in Figure 5.

$$\frac{\partial^2 T}{\partial x^2} = \frac{\left[T^P_{(m-1, n)} + T^P_{(m+1, n)} - 2T^P_{(m, n)}\right]}{\Delta x^2} \tag{4}$$

$$\frac{\partial^2 T}{\partial y^2} = \frac{\left[T^P_{(m, n-1)} + T^P_{(m, n+1)} - 2T^P_{(m, n)}\right]}{\Delta y^2} \tag{5}$$

$$\frac{\partial T}{\partial t} = \frac{\left[T^{P+1}_{(m, n)} - T^P_{(m, n)}\right]}{\Delta t} \tag{6}$$
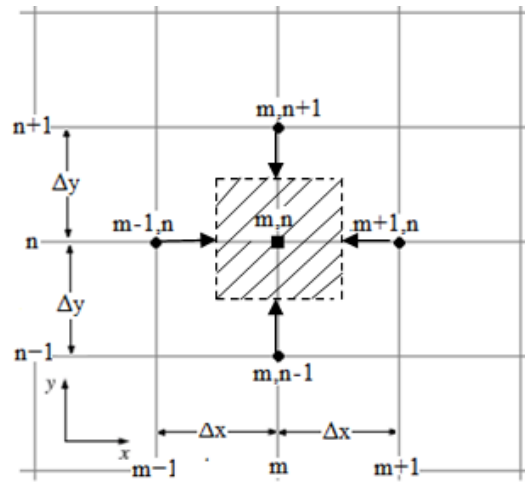
Figure 5. Interior nodes configuration

Substituting Equations (4), (5) & (6) into Equation (3), we get the governing two-dimensional transient conduction heat transfer equation for interior nodes:

$$T^{P+1}_{m,n} = F_o\left(T^P_{m-1,n} + T^P_{m+1,n} + T^P_{m,n-1} + T^P_{m,n+1}\right) + (1 - 4F_o)T^P_{m,n} \tag{7}$$

where, $\Delta x = \Delta y = \Delta s$ (Equally spacing). $F_o = \alpha \times \Delta t / \Delta s^2$,

Fourier number dimensionless parameter.

The stability criteria of Equation (7) are maintained as long as ($F_o \leq 0.25$) or ($\alpha_i \leq 2.5 \times 10^{-7}$ m^2/sec).

According to Kumar [20], in a moderate case heating scenario, MCHS, where the effect of linear convection and radiation is combined into an equivalent non-linear convection term:

$$h\,(T_f + T_s)^N = h(T_f + T_s)\ + \varepsilon\,\sigma\big(\overline{T_f^4} + \overline{T_{fs}^4}\big) \tag{8}$$

The mild exposure principle from the literature [20], MCHS, is adopted to determine the column expose surface temperature, T_s.

Figure 6 shows that the corner surface fire exposed node is subjected to convection, radiation from the bottom and left-hand sides, and conduction from the top and right sides.

Combined equivalent (Convection and Radiation) term + Conduction term = $\rho C_p \dfrac{\partial T}{\partial t}$ Transient term
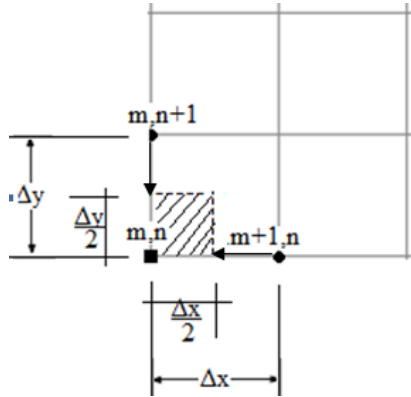
Figure 6. Corner surface node configuration.

$$T_{m,n}^{P+1} = \frac{2\,\Delta t\,\alpha}{\Delta s^2}\left[\frac{2\,\Delta s\,h_f}{K}\big(T_f^P - T_{m,n}^P\big)^N + \big(T_{m+1,n}^P + T_{m,n+1}^P\big)\right] + \left(1 - \frac{4\,\Delta t\,\alpha}{\Delta s^2}\right)T_{m,n}^P \tag{9}$$

Figure 7 shows that the bottom surface fire exposed node is subjected to convection and radiation from the bottom side and conduction from the top, right and left sides.
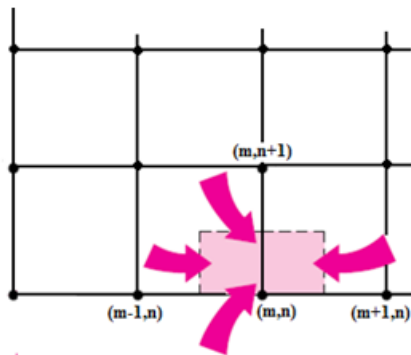
Figure 7. Bottom surface node configuration.

$$T_{m,n}^{P+1} = \frac{\Delta t\,\alpha}{\Delta s^2}\left[\frac{2\,\Delta s\,h_f}{K}\big(T_f^P - T_{m,n}^P\big)^N + \big(T_{m-1,n}^P + T_{m+1,n}^P\big) + 2T_{m,n+1}^P\right] + \left(1 - \frac{4\,\Delta t\,\alpha}{\Delta s^2}\right)T_{m,n}^P \tag{10}$$

Figure 8 shows that the side surface fire exposed node is subjected to convection and radiation from the left-hand side and conduction from the top, right and bottom sides.
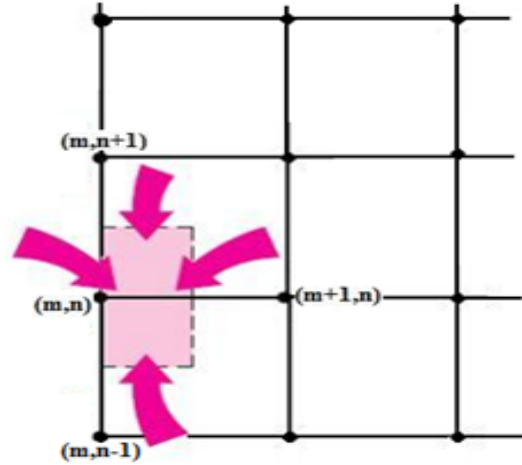
Figure 8. Side surface node configuration.

$$T_{m,n}^{P+1} = \frac{\Delta t\,\alpha}{\Delta s^2}\left[\frac{2\,\Delta s\,h_f}{K}\big(T_f^P - T_{m,n}^P\big)^N + \big(T_{m,n-1}^P + T_{m,n+1}^P\big) + 2T_{m+1,n}^P\right] + \left(1 - \frac{4\,\Delta t\,\alpha}{\Delta s^2}\right)T_{m,n}^P \tag{11}$$

Kumar [20] proposed the simplest form of thermal diffusivity as a function of temperature:

$$\alpha_t = \frac{1.45}{(T + 400)},\quad \text{m}^2/\text{hr} \tag{12}$$

Initial, t = 0 and temperature $T_i = 20$ °C. Therefore, $\alpha_T = 9.58 \times 10^{-7}$ m^2/sec, consequently this value violates the stability criteria of the adopted FD numerical method to solve Equation (7). Hence, the constants 1.45 and 400 in Equation (12) will be examined and refined to suit the thermal analysis and minimize the difference between experimental data and the thermal simulation model output.

2.4 Boundary and Initial Conditions

The reinforcement steel bars will be neglected in the thermal analysis, because they represent only 2.45% of the gross cross-sectional area of the column. Hence the material of the column was considered wholly concrete as homogenous in the thermal branch.

The subjected HSCC cross-sectional area at the mid-height is divided into four segments by two symmetry lines (double symmetric shape), only a quarter of the section is analyzed. It was equally spaced into a sufficient number of nodes, $\Delta x = \Delta y$ each representing a square millimeter of the column's cross-sectional area, with two

perpendicular hot air-surrounded surfaces and the other two perpendicular surfaces representing the boundary symmetry lines.

There are four boundary conditions at the *x* and *y* directions (two at the fire-exposed surfaces and two at the symmetry lines) and one initial condition at τ= 0. These are:

$$T(x, y, 0) = T_i = 20°C, \quad T(x, 0, t) = T_s(x, 0, t),$$
$$T(0, y, t) = T_s(0, y, t)$$

$$T(W/2, y, t) = \frac{[T(x_{m+1}, y, t) + T(x_{m-1}, y, t)]}{2}$$

$$T(x, D/2, t) = \frac{[T(x, y_{n+1}, t) + T(x, y_{n-1}, t)]}{2}$$

After that, the model will be ready for another step forward, in other words; correlations of remaining strengths for both steel reinforcement and concrete from the existing literature will be introduced to determine the strength reduction of both materials during the fire exposure scenario.

Muhammad Yaqub et al. [18], proposed the following correlations (13) and (14) to measure the effect of elevated temperature on the HSCC strength for both concrete and reinforcement bars.

To calculate the steel bars remaining strength:

$$\xi_{st} = \kappa + \frac{1-\kappa}{1+\left(\frac{T}{T_1}\right)+\left(\frac{T}{T_2}\right)^2+\left(\frac{T}{T_8}\right)^8+\left(\frac{T}{T_{64}}\right)^{64}} \quad (13)$$

where, ξ_{st} is the ratio between the remaining compressive strength at temperature T °C and the original unheated compressive strength of reinforcing steel bars at 20 °C. κ, T_1, T_2, T_8, and T_{64}, are given tabulated parameters for various types of steel.

To calculate the concrete remaining strength:

$$\xi_{st} = \kappa + \frac{1-\kappa}{1+\left(\frac{T}{T_1}\right)+\left(\frac{T}{T_2}\right)^2+\left(\frac{T}{T_8}\right)^8+\left(\frac{T}{T_{64}}\right)^{64}} \quad (14)$$

where, ξ_c is the ratio between the remaining compressive strength at temperature T °C and the original unheated compressive strength of concrete at 20 °C. T_1, T_2, T_8, and T_{64}, are given tabulated parameters for various types of aggregates.

The types of steel most often used in building design and construction is either hot-rolled or cold-drawn, with a modulus of elasticity of about 210 GPa at 20 °C [12-14].

The specifications of steel bars 400 MPa compression yield strength (25 mm diameter), from literature by Kodur et al. [17] were used to evaluate the performance of HSCC in a fire.

As shown in Table 1, Euro-code classified HSC into three classes, depending on its Cylinder / Cube compressive strength [12]:

Table 1. HSC Euro-code classifications

Classification	Minimum GPa	Maximum GPa
Class 1	55 / 67	60 / 75
Class 2	70 / 85	80 / 95
Class 3	90 / 105	Higher

The effects of temperature on the elastic modulus of concrete and the reinforcing bars are proposed in the literature [21]. Equation (15) showed the ratio of the reinforcing bars' modulus of elasticity at elevated temperature to the reinforcing bars' modulus of elasticity at room temperature.

$$\frac{E_{st,T}}{E_{st,20\,C^0}} = \begin{cases} 1+\frac{T}{\left[2000\times\ln\left(\frac{T}{1100}\right)\right]}, & for\ 0°C < T \le 600°C \\ 690\times\frac{\left(1-\frac{T}{1000}\right)}{(T-53.5)}, & for\ 600°C < T \le 1000°C \end{cases} \quad (15)$$

The modulus of elasticity of concrete also decreases as temperature increases [21]. Equation (16) showed the reduction ratio of concrete modulus of elasticity due to temperature increase.

$$\frac{E_{c,T}}{E_{c,20\,C^0}} = \begin{cases} 1, & for\ T < 150°C \\ \frac{(700-T)}{550}, & for\ T \ge 150°C \end{cases} \quad (16)$$

The concrete modulus of elasticity at room temperature may fall within a very wide range, 5 to 50 GPa.

Table 2, shows reinforced concrete elasticity moduli at room temperature based on the type of aggregate of the reinforced concrete [12-14]:

Table 2. Concrete Modulus of elasticity at 20 °C

Type of aggregate	Modulus of elasticity $E_{C, 20°C}$
Carbonate aggregate	34 GPa
Silicate aggregate	38 GPa
Light weight aggregate	19 GPa

Kang Hai Tan [3] proposed the Rankine formula correlations, Equations (17) to (19), to predict the failure load of the reinforced concrete column under fire conditions.

$$\frac{1}{P_{R(t)}} = \frac{1}{u_{pr}\times P_{p(t)}} + \frac{1}{P_{e(t)}} \quad (17)$$

$$P_{p(t)} = \beta_{c(t)}\,f'_{c(0)}\,A_C + \beta_{yr(t)}\,f_{y(0)}\,A_{st} \quad (18)$$

$$P_{e(t)} = \frac{\pi^2\left[\beta_{Ec(t)}\,0.2\,E_{c(0)}\,I_c + \beta_{Est(t)}\,E_{sr(0)}\,I_{st}\right]}{L_e^2} \quad (19)$$

where,

$P_{R(t)}$: Predicted failure load by Rankine formula.

$P_{p(t)}$: Plastic squashing load of RCC at time **t**.

$P_{e(t)}$: Elastic buckling load of RCC at time **t**.

.t: Fire exposure time.

A_c: Column concrete cross-section area.

A_{st}: Column reinforcing steel cross-section area.

.$f_c^{'}$: Concrete cylinder compression strength.

f_y: Steel reinforcement yield strength.

E_c: Concrete elastic modulus.

E_{st}: Steel reinforcement elastic modulus.

I_c: Concrete 2nd moment of area.

I_{st}: Steel reinforcement 2nd moment of area.

L_e: Column effective length.

.c: Column concrete covering in mm.

Concert strength reduction factor in fire:

$$\beta_{c(t)} = \frac{\gamma_{(t_e)}}{\sqrt{1 + \left(0.3\, A_c^{-0.5}\, t_e\right)^{A_c^{-0.25}}}} \qquad (20)$$

Steel strength reduction factor in fire:

$$\beta_{yr(t)} = \gamma_{(t_e)} \left(1 - \frac{0.9\, t_e}{0.046\, c + 0.11}\right) \geq 0 \qquad (21)$$

$$\gamma_{(t_e)} = 1 - 0.3\, t_e \geq 0.85, \quad t_e = \alpha_{agg} \times \alpha_{ISO} \times t \qquad (22)$$

$$\alpha_{agg} = \left\{ \begin{array}{c} 1 \text{ for siliceous aggregate} \\ 0.9 \text{ for carbonate aggregate} \end{array} \right\}, \text{ and}$$

$$\alpha_{ISO} = \left\{ \begin{array}{c} 1 \text{ for ISO 834 Standard fire} \\ 0.85 \text{ for ASTM} - \text{E119 Standard fire} \end{array} \right\} \qquad (23)$$

2.5 Model Flow Chart

Figure 9 shows the model flow chart of the numerical thermal simulation and mechanical performance evaluation of the subjected HSCC based on the adopted MCHS in a fire.
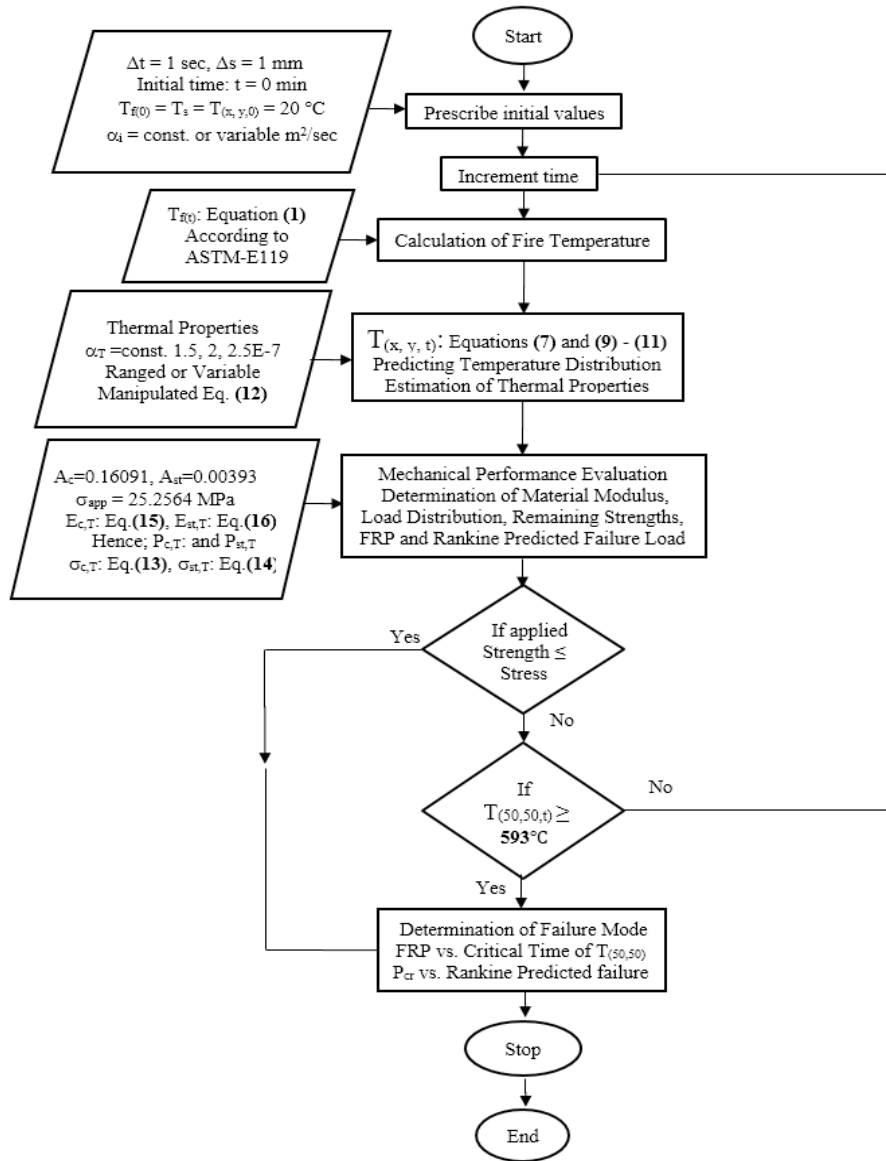
Figure 9. Flow chart of the MCHS numerical simulation model

3. Results

The main findings of this study are presented in this section. They are laid out in three main subsections. The thermal simulation (temperature distribution) and model prediction validation, statistical error analysis for testing the model prediction accuracy, and the mechanical performance evaluation of the subjected HSCC fire response characteristics of constituent.

3.1 General Behavior of the Model

In the first subsection, the temperature distribution in the cross-sectional area at mid-height of the subjected HSCC is determined according to the adopted MCHS with constant, ranged, and variable thermal diffusivities in a fire. The temperature distribution at different depths is validated by experimental data from the literature.

Figure 10a shows the temperature distribution in MCHS with constant concrete thermal properties: $\alpha = 2.5 \times 10^{-7}$ m^2/sec, $k = 1.5$ W/(m-^{o}C), combined heat transfer coefficient: $h_f = 15$ W/(m^2-^{o}C), and combined heat transfer exponent: $N = 1.55$.

One observation that can be made is that as the time interval increases, so does the temperature of the concrete column. Logically, this is because as more time passes, a greater quantity of heat would enter the column thus elevating its temperature.

Figure 10b shows that the thermal diffusivity ($\alpha = 2.5 \times 10^{-7}$ m^2/sec) is suitable for predicting the temperature distribution of nodes at 76 mm depth only, overestimates temperature for nodes at 13, 32, and 50 mm depths, and underestimates temperature for nodes deeper than 76 mm.
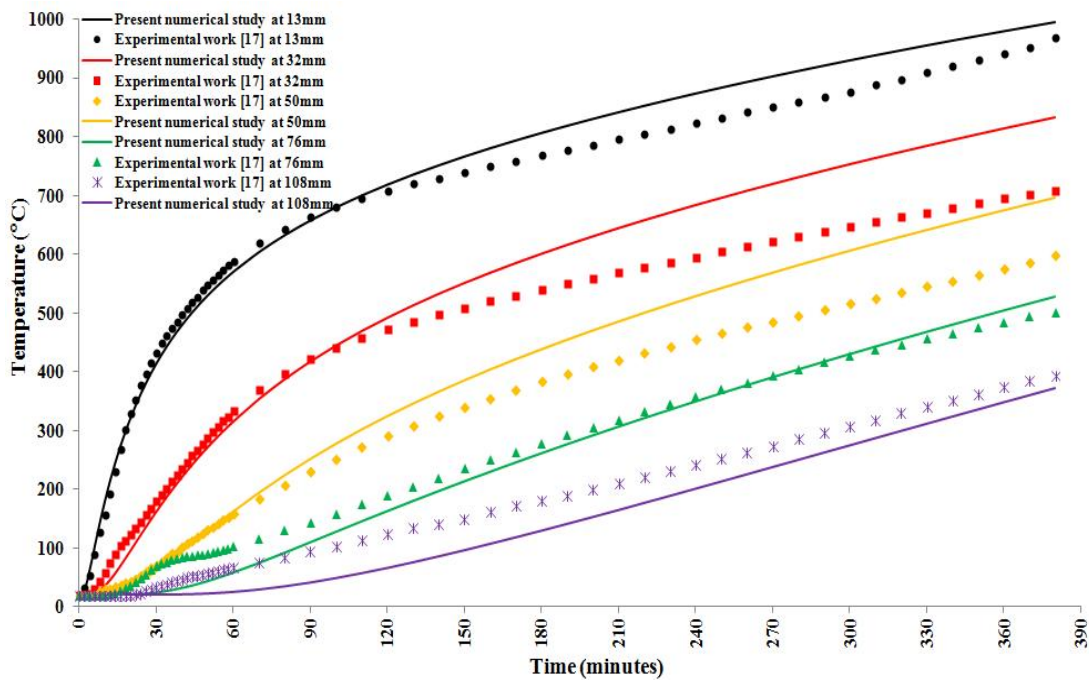
a
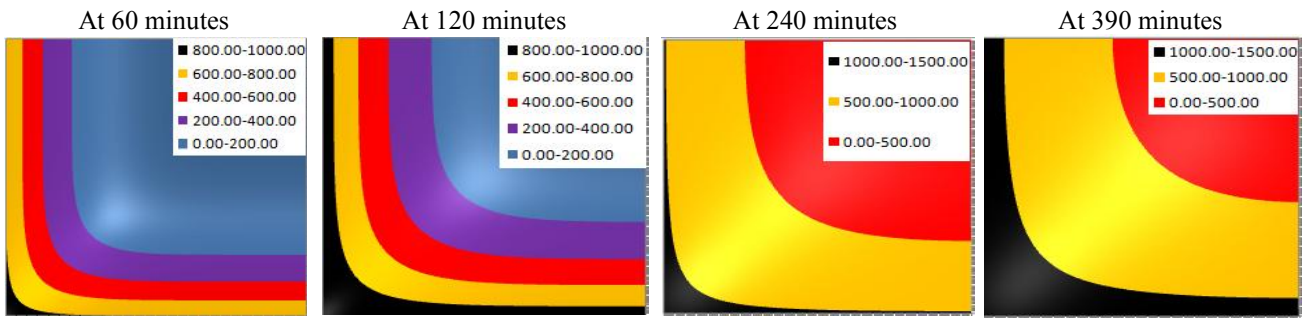
b

Figure 10. a) MCHS Temperature distribution with $\alpha = 2.5 \times 10^{-7}$ m^2/sec at 13, 32, 50, and 76 mm depths VS time and against the related previous experimental test results. b) Temperature contour of MCHS with 2.5×10^{-7} m^2/sec thermal diffusivity.

Figures 11a and 11b show temperature distribution and contour in MCHS with constant concrete thermal properties: $\alpha = 2.0 \times 10^{-7}$ m²/sec, k = 1.5 W/(m-°C), combined heat transfer coefficient: h_f = 15 W/(m²-°C), and combined heat transfer exponent: N = 1.55.

Figure 11a shows that the thermal diffusivity ($\alpha = 2.0 \times 10^{-7}$ m²/sec) is suitable for predicting the temperature distribution of nodes at 50 mm depth only, overestimates temperature at 13, and 32 mm, and underestimates temperature for nodes deeper than 50 mm.

Figures 12a and 12b show temperature distribution and contour in MCHS with constant concrete thermal properties: $\alpha = 1.5 \times 10^{-7}$ m²/sec, k = 1.5 W/(m-°C), combined heat transfer coefficient: h_f = 15 W/(m²-°C), and combined

heat transfer exponent: N = 1.55.

Figure 12a shows that the thermal diffusivity ($\alpha = 1.5 \times 10^{-7}$ m²/sec) is suitable for predicting the temperature distribution of nodes at 13, and 32 mm depths after 180 minutes of fire exposure only, and underestimates temperature for all nodes at all times. (Lower value of thermal diffusivity is more suitable particularly for the closer nodes to the fire-exposed surfaces and vice versa).

The fluctuation of nodal temperatures with the change of thermal diffusivity during the increase of fire temperature is solid evidence that led to the first conclusion which confirms that the material properties are not constants but functions of temperatures, depths and fire time.
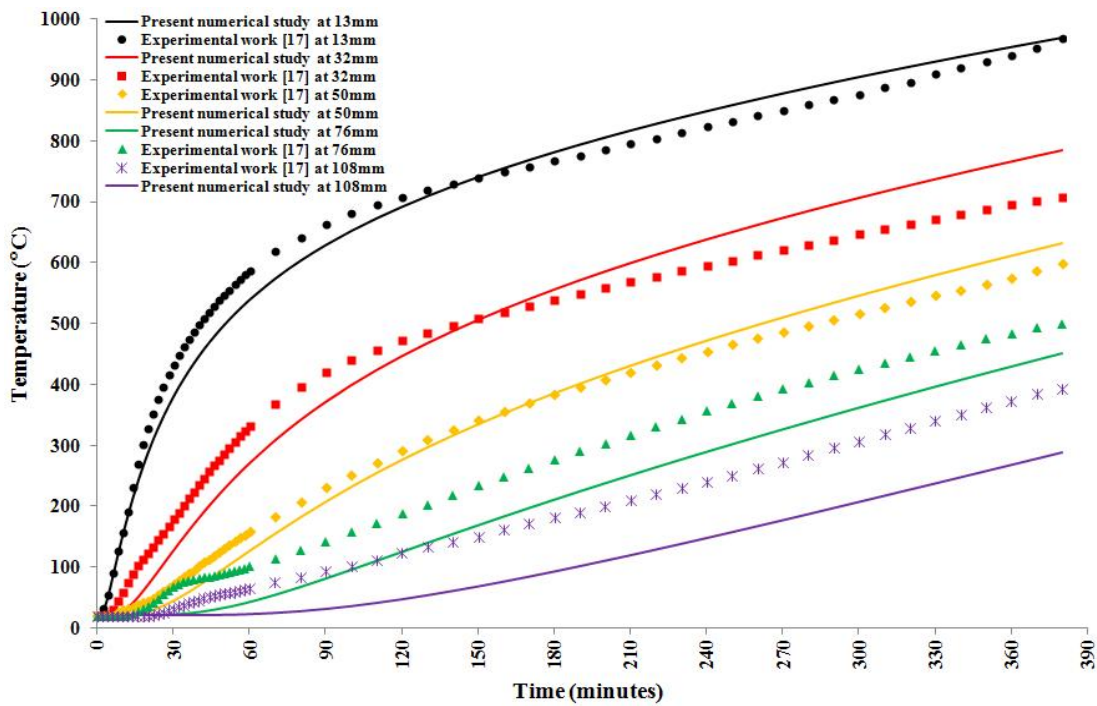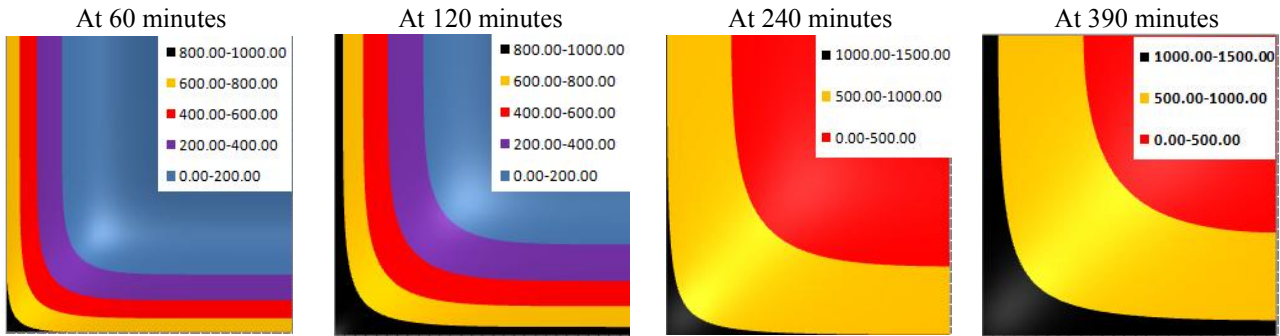
Figure 11. a) MCHS Temperature distribution with $\alpha = 2.0 \times 10^{-7}$ m²/sec at 13, 32, 50, and 76 mm depths VS time and against the related previous experimental test results. b) Temperature contour of MCHS with 2.0×10^{-7} m²/sec thermal diffusivity.
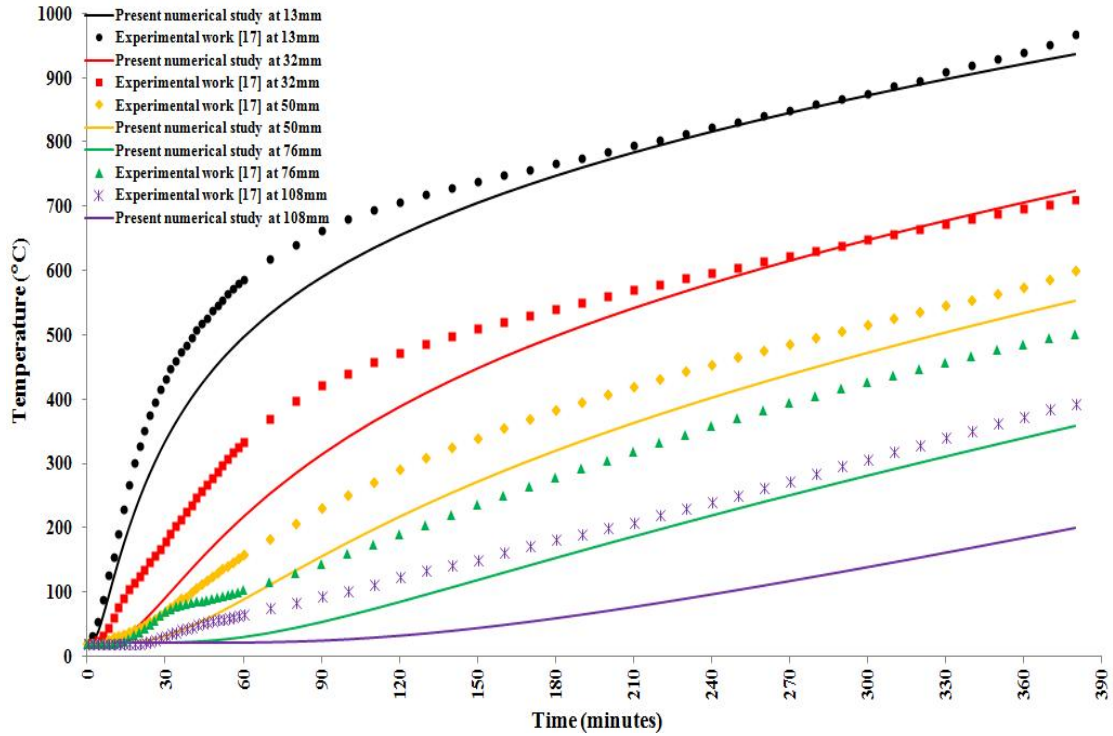
a
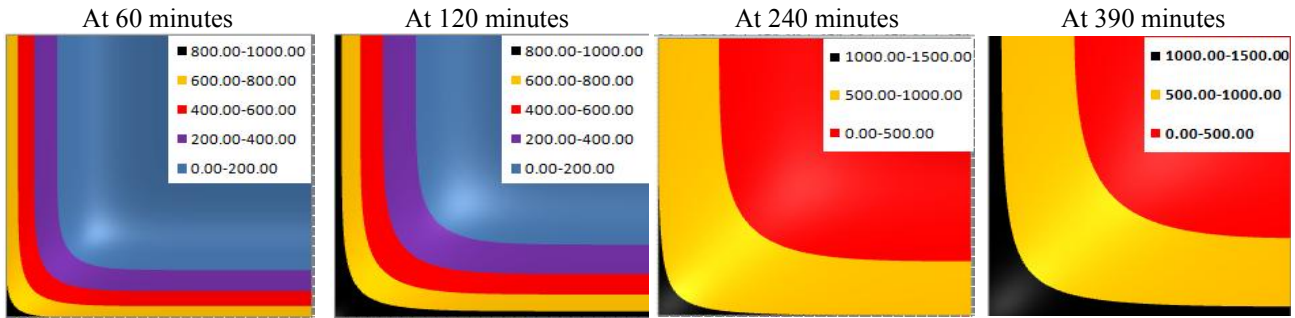
b

Figure 12. a) MCHS Temperature distribution with $\alpha = 1.5 \times 10^{-7}$ m^2/sec at 13, 32, 50, and 76mm depths VS time and against the related previous experimental test results. b) Temperature contour of MCHS with 1.5×10^{-7} m^2/sec thermal diffusivity.

Constants in the proposed correlation of thermal diffusivity [12], Equation (12), were examined and manipulated to form a function of temperature and time that suit the thermal temperature distribution and minimizes the difference between experimental data and numerical model output.

$$\alpha_{i,j,t} = A \times \frac{e^{\left(-B \times \text{time}\right)}}{\left(3600 \times (T + 400)\right)},$$

where;

A: $0.75 - 0.875$

B: $0.0006 - 0.0001$

For spacing ranges
$0 - 16$ mm
$20 - 36$ mm
$40 - 56$ mm
$60 - 76$ mm
$80 - 96$ mm
$100 - 203$ mm

Figure 13a shows that the model temperature distribution output is improved when introducing the thermal diffusivity as a function of temperature and time that varies for each layer of depth.

The resulting manipulated correlation of the ranged
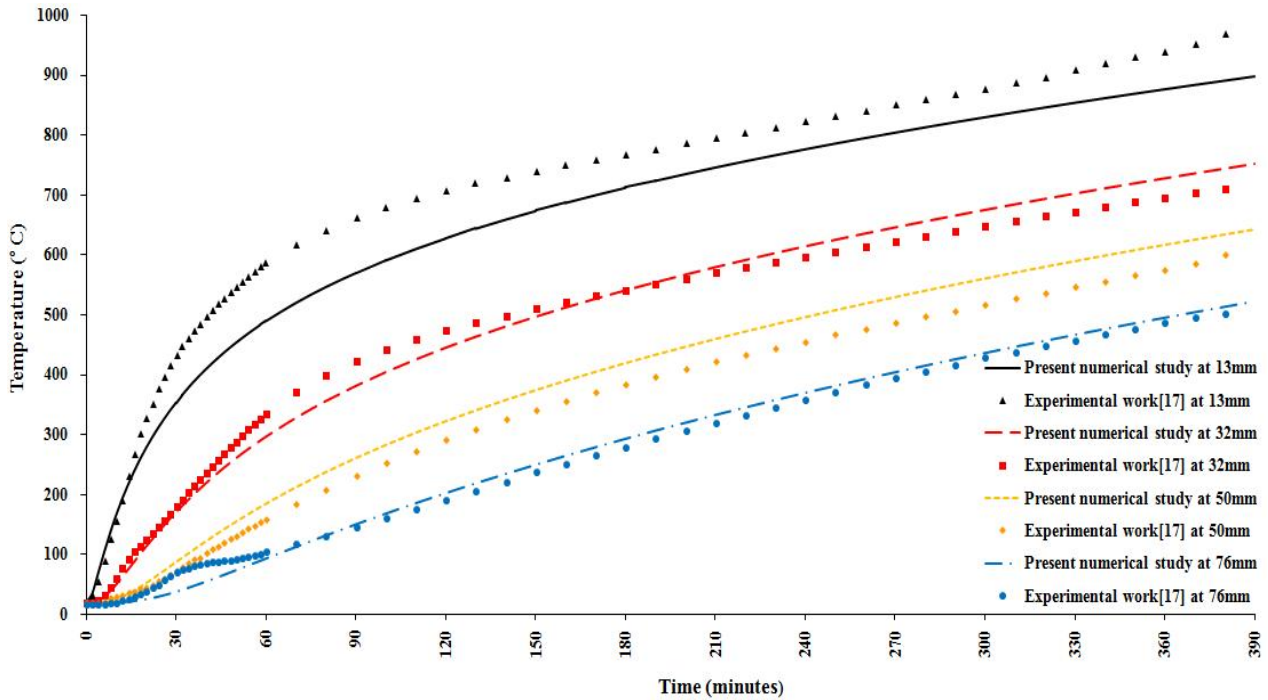
a
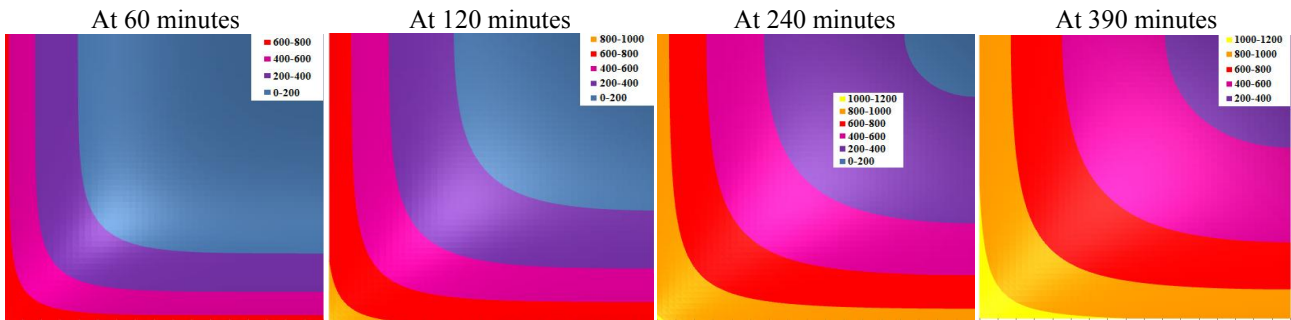
b

Figure 13. a) MCHS Temperature distribution with ranged thermal diffusivity at 13, 32, 50, and 76 mm depths VS time and against the related previous experimental test results. b) Temperature contour of MCHS with ranged thermal diffusivity.

thermal diffusivity that generates temperature distribution in Figure 13a was refined to be a function of temperature, time, and depth, in other words a correlation for all layers instead of one correlation for each layer of depth.

$$\alpha_{i,j,t} = 0.01 \sqrt{(x^2 + y^2)} \frac{e^{(-0.1 \times \text{time}/60)}}{\left(3600 \times (T_{i,j,t} + 400)\right)}, \quad m^2/\text{Sec.}$$

where; $\begin{Bmatrix} x_i \text{ and } y_j \text{ in mm} \\ \text{time in minutes} \\ T \text{ in } °C \end{Bmatrix}$

Figure 14a shows that the temperature distribution accuracy was not fully improved by using the variable thermal diffusivity compared with Figure 13a which showed

the temperature distribution when introducing the ranged thermal diffusivity.

Figures 10a, 11a, 12a, 13a, and 14a show the resulted model temperature distribution when using constant ((1.5, 2.0, and 2.5)×10^{-7}), ranged, and variable thermal diffusivities (m^2/sec), they also show that the validation of model output results for every case by comparing the model predictions with the related previous experimental data from the literature.

3.2 Test Model Prediction Accuracy

In the second subsection, the model predictions accuracy is tested by conducting a statistical error analysis
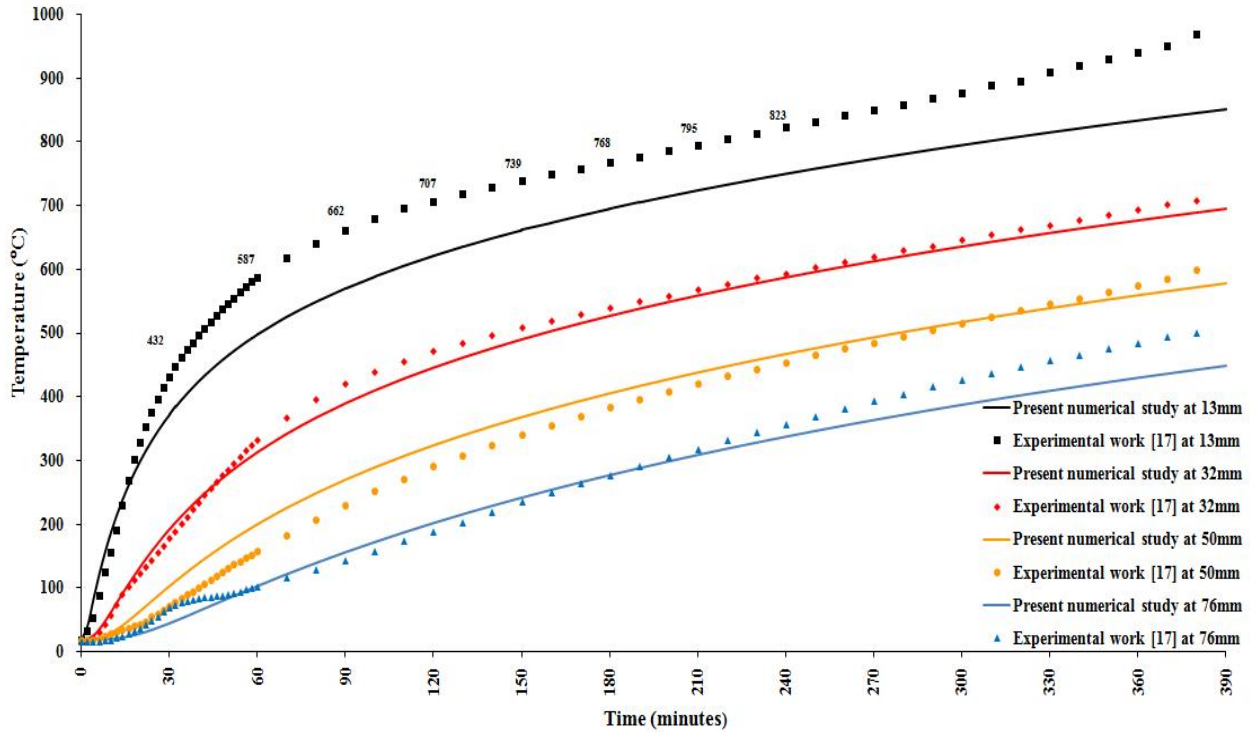
a
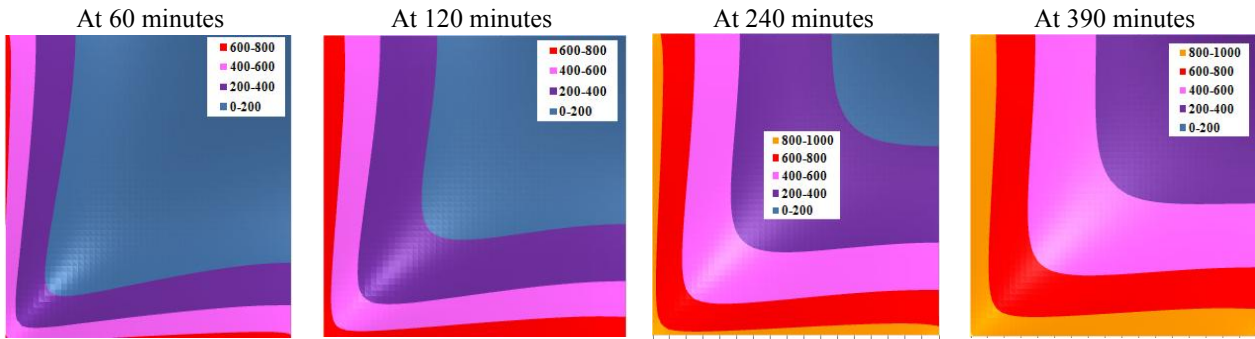
b

Figure 14. a) MCHS Temperature distribution with variable thermal diffusivity at 13, 32, 50, and 76mm depths VS time and against the related previous experimental test results. b) Temperature contour of MCHS with variable thermal diffusivity.

including:

1) Mean percentage error, (MPE), provides information on the mean percentage error of the predicted readings about the actual reading or experimental data [22].

$$MPE = \left\{ \sum \left[\frac{(T_{exp} - T_t)}{T_{exp}} \times 100 \right] \right\} / n$$

2) Mean bias error, (MBE), provides information with respect to overestimation or underestimation (A low MBE value is desired) and (A positive value of MBE gives an overestimation in the predicted data and vice versa) [22].

$$MBE = \left[\sum (T_t - T_{exp}) \right] / n$$

3) Root mean square error, (RMSE). The lower the RMSE, the more accurate the model is. The sign of percentage errors is neglected [22].

$$RMSE = \left\{ \left[\sum (T_t - T_{exp})^2 \right] / n \right\}^{1/2}$$

where,

T_{exp}: the reference experimental temperatures.

T_t: the model numerical temperatures.

n: number of temperature readings.

43

Tables 3-5 show the mean percentage error, the mean bias error, and the root mean square error of the MCHS model output temperatures for nodes at different depths when compared with related experimental data from the literature according to the key model parameters as shown below:

The lower MPE for nodes at 13 mm: $MPE_{13} = 4.14\%$ when using ranged thermal diffusivity.

The lower MPE for nodes at 32 mm: $MPE_{32} = 3.78\%$ when using ranged thermal diffusivity.

The lower MPE for nodes at 50 mm: $MPE_{50} = 13.62\%$ when thermal diffusivity $= 2.5 \times 10^{-7}$.

For the ranged thermal diffusivity: $MPE_{50} = 16.28\%$.

The lower MPE for nodes at 76 mm: $MPE_{76} = 6.73\%$ when using variable thermal diffusivity.

For the ranged thermal diffusivity: $MPE_{76} = 8.58\%$.

The accurate RMSE for nodes at 13 mm: $RMSE_{13} = 25.97\ ^\circ C$ when using ranged thermal diffusivity.

The accurate RMSE for nodes at 32 mm: $RMSE_{32} = 13.72\ ^\circ C$ when using ranged thermal diffusivity.

The accurate RMSE for nodes at 50 mm: $RMSE_{50} = 24.36\ ^\circ C$ when thermal diffusivity $= 2.0 \times 10^{-7}$.

For the ranged thermal diffusivity: $RMSE_{50} = 32.57\ ^\circ C$.

The accurate RMSE for nodes at 76 mm: $RMSE_{76} = 19.71\ ^\circ C$ when using ranged thermal diffusivity.

Table 3. Accuracy statistical error analysis of MCHS temperature distribution with constant thermal diffusivity.

	MPE %			MBE °C			RMSE °C		
Constant α: $\times 10^{-7}$ (m^2/sec)$\Rightarrow$	2.5	2.0	1.5	2.5	2.0	1.5	2.5	2.0	1.5
T-01 at 13 mm from the surface	4.79	6.07	12.39	13.38	−14.08	−50.92	30.25	33.44	62.54
T-02 at 32 mm from the surface	13	17.68	25.35	26.98	−9.23	−54.66	60.17	48.54	70.03
T-11 at 50 mm from the surface	13.62	16.67	29.49	29.43	−6.14	−48.29	50.19	24.36	52.99
T-03 at 76 mm from the surface	19.83	31.21	43.30	−13.70	−44.52	−78.37	21.67	50.91	95.78
The average values: $\Rightarrow$	12.81	17.90	27.63	14	−18.49	−58.06	40.57	39.31	70.33

Table 4. Accuracy statistical error analysis of MCHS temperature distribution with ranged thermal diffusivity.

$\alpha_{i,j,t} = A \times \dfrac{e^{\left(-B \times time\right)}}{\left(3600 \times (T + 400)\right)}$	MPE %	MBE °C	RMSE °C
T-01 at 13 mm from the surface	4.14	0.88	25.97
T-02 at 32 mm from the surface	3.78	4.43	13.72
T-11 at 50 mm from the surface	16.28	23.93	32.57
T-03 at 76 mm from the surface	8.58	11.85	19.71
The average values: $\Rightarrow$	8.19	10.27	22.99

Table 5. Accuracy statistical error analysis of MCHS temperature distribution with variable thermal diffusivity.

$\alpha_{i,j,t} = 0.01 \sqrt{(x^2 + y^2)} \dfrac{e^{\left(-0.1 \times time/60\right)}}{\left(3600 \times (T_{i,j,t} + 400)\right)}$	MPE %	MBE °C	RMSE °C
T-01 at 13 mm from the surface	13.02	−63.34	73.75
T-02 at 32 mm from the surface	4.08	−7.06	14.28
T-11 at 50 mm from the surface	17.36	19.30	26.72
T-03 at 76 mm from the surface	6.73	−7.36	21.45
The average values: $\Rightarrow$	10.29	−14.61	34.05
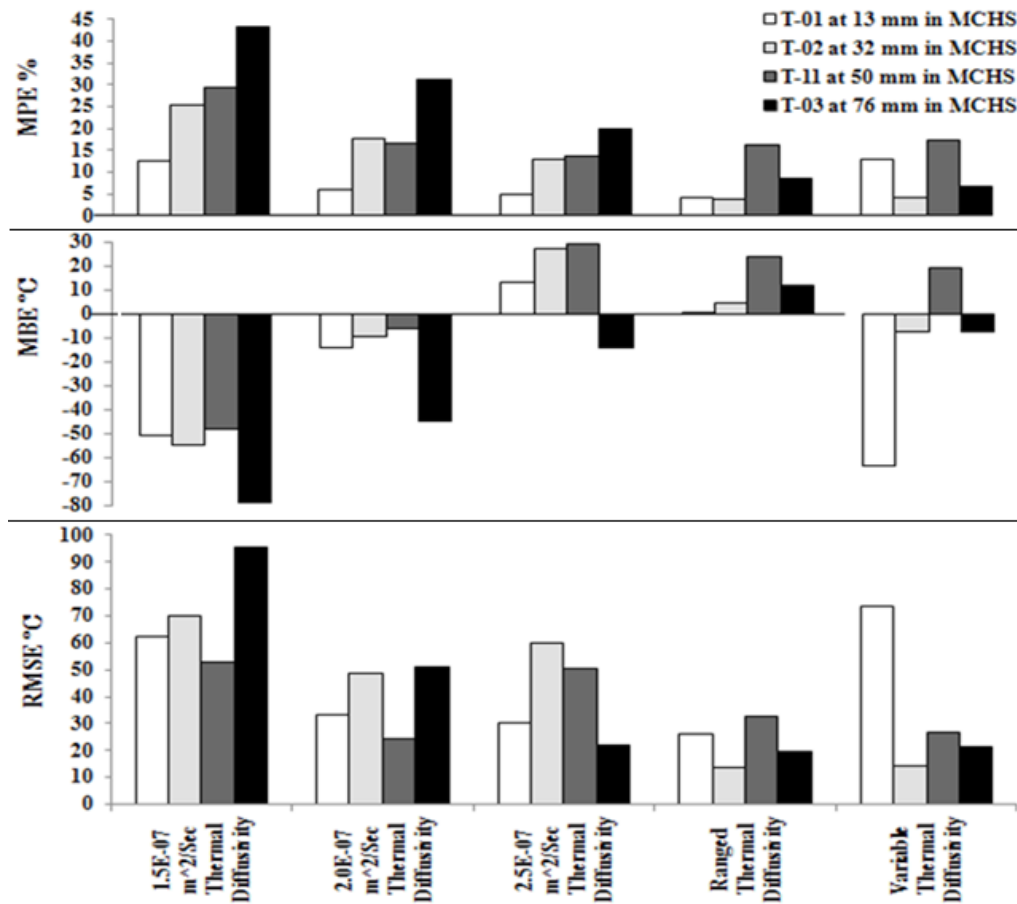
Figure 15. Statistical error analysis for testing the accuracy of MCHS temperature distributionmodel output.

Figure 15 shows the statistical error analysis charts that present illustration and comparison to test the accuracy of the temperature distribution model output in MCHS with constant, ranged, and variable thermal diffusivities for nodes at different depths.

As shown in Figure 15, the lower RMSE and MBE values in the MCHS temperature distribution model output for the vast majority of nodes which represent the accurately predicted model results that are compared with related experimental data are achieved when using the ranged thermal diffusivity.

Furthermore, the averaged minimum MBE in MCHS corresponding to model output overestimation and underestimation is achieved for the vast majority of nodes by using ranged thermal diffusivity. The overall model accuracy is confirmed by the averaged minimum MPE % of all temperature nodes.

3.3 Characteristics of Response and Mechanical Performance Evaluation

The third subsection, finally, evaluates mechanical performance of the subjected HSCC fire response characteristics of constituent including:

1) Determining combined thermal properties at different depths for the subjected HSCC in a fire.

The main HSCC constituent materials response due to fire is the change in combined thermal properties (thermal diffusivities in m^2/sec). The adopted correlated thermal diffusivity MCHS model results are used to illustrate the change of thermal diffusivity as a function of temperature, time, and depth that varies for each node.

2) Determining the HSCC mechanical properties such as elasticity moduli, remaining strengths, and load distribution during the fire for both concrete and reinforcing steel.

In this paper, the Compression Strength and the Modulus of Elasticity for both steel reinforcement and concrete were considered as the mechanical performance criteria when evaluating the mechanical properties of the subjected HSCC in a fire.

The interface corner temperature of the node at 50 mm from the fire-exposed surfaces that resulted from a thermal branch of the model was used to calculate the remaining strengths according to Equations (13) and (14) for both

concrete and reinforcing steel bars.

Load distribution between steel reinforcement and concrete based on (MCHS). Basically, if a column of two different materials is subjected to a temperature rise under an axial load, at a certain temperature one of those materials will carry the total load [11,23].

3) Determining the subjected HSCC Rankine predicted failure load in the fire.

The proposed Rankine formula [15], according to Equations (17) to (23), assumes a linear interactive relationship between two failure modes of RCCs in a fire, these two modes are:

(1) **Crushing** for short columns (plastic squashing load causes compression failure).

The column is assumed to be short if the slenderness ratio is less than unity.

(2) **Buckling** for slender columns (elastic buckling load causes buckling failure).

The column is assumed to be slender (long) if the slenderness ratio is greater than unity.

For columns in the intermediate range where the slenderness ratio is close to unity, the failure occurs because the two modes, compression failure, and buckling failure, will interact with each other.

The subjected HSCC Rankine predicted failure load in the fire is calculated according to proposed correlations (17) to (23) by introducing the interface corner temperature that resulted from MCHS with ranged thermal diffusivity.

Figure 16a shows the change in combined thermal properties (thermal diffusivities in m^2/sec) at different depths versus time for the adopted MCHS when introducing ranged thermal diffusivity as a function of temperature and time that varies for each layer of depth.

a

b
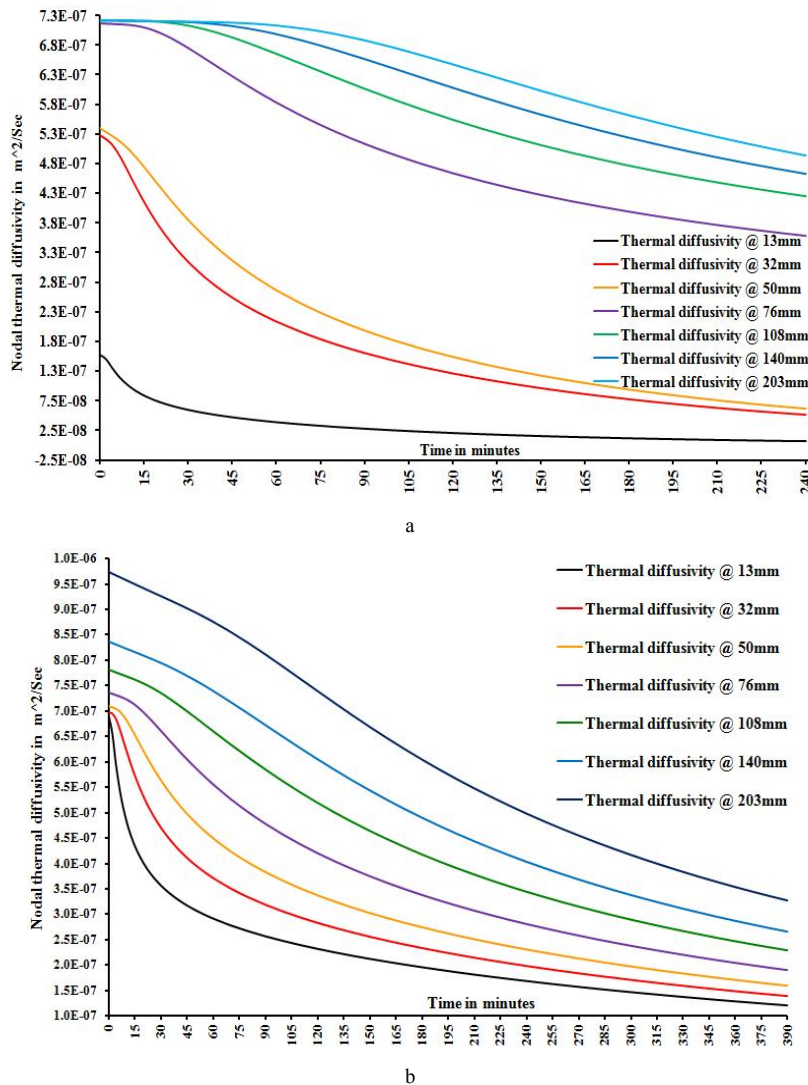
Figure 16. a) The change in ranged thermal diffusivities verses time for each layer of depth. b) The change in variable thermal diffusivities verses time for each node of depth.

Figures 16a and 16b show that the variation in the thermal diffusivity is solid evidence that proves that thermal and physical properties (K, Cp & p) of tested material HSC have to be changed.

Figures 17a and 17b show that the compression strength of concrete and compression strength of reinforcing steel bars are decreasing due to temperature increase because of fire exposure, on a base of interface corner node critical temperature MCHS model results when the thermal diffusivity is ranged versus corner critical interface temperature and time comparing with theoretical correlations proposed for RC under fire in reference [1].

The model predicted interface corner temperature was used in Equations (15) and (16) to determine the effective elastic moduli for both steel bars and concrete as shown below figures.

Figures 18a and 18b show the reduction in reinforcement steel and concrete elasticity moduli due to temperature increase because of fire exposure, based on interface corner critical temperature MCHS model results when the thermal diffusivity is constant, ranged, and variable versus time.
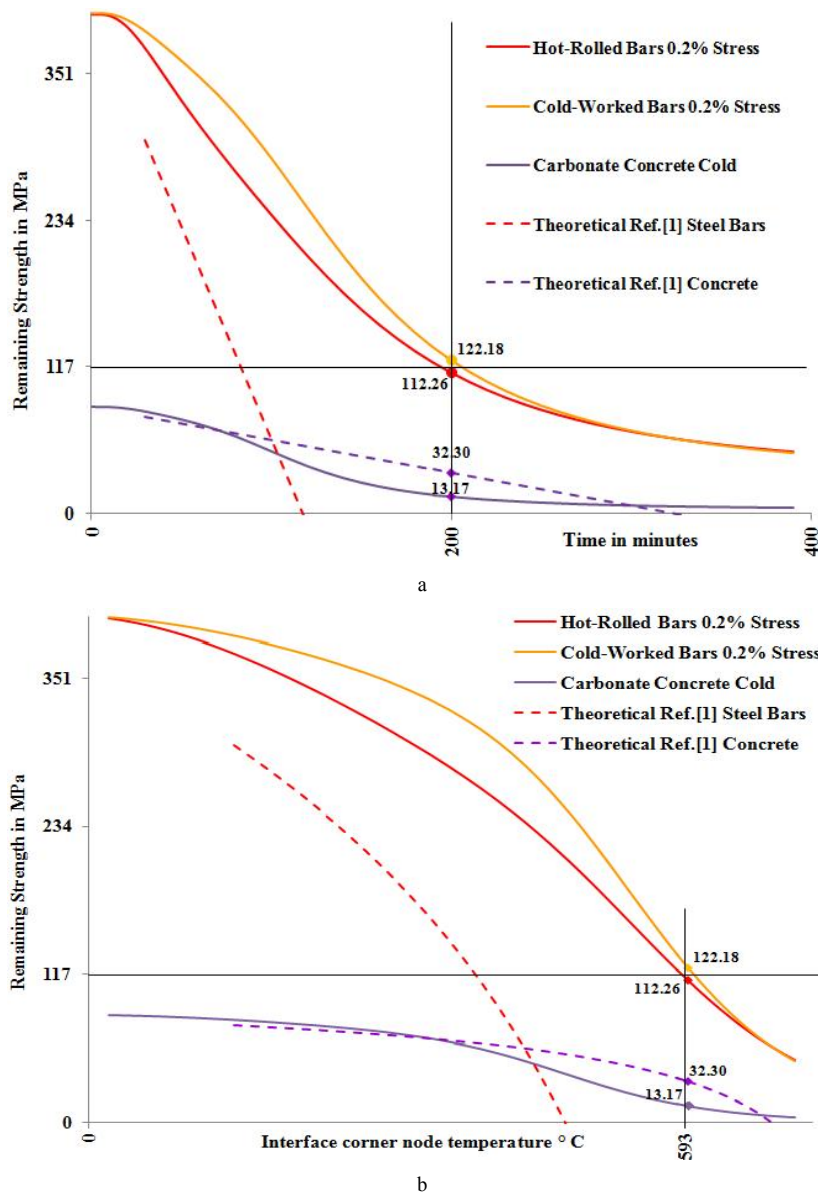
Figure 17. a) MCHS with ranged thermal diffusivity remaining strength VS time at interface-corner node. b) MCHS with ranged thermal diffusivity remaining strengths VS temperature at interface-corner node.

The time steps of model predicted middle and corner interface temperatures were used in Equations (17) ~ (23) to determine Rankine predicted failure load of RCC verses interfaces temperatures for the subjected HSCC in a fire exposure compared with the design load capacity of the subjected HSCC.

Figures 20a shows the load increase on reinforcing steel bars and the load decrease on concrete due to temperature increase because of fire exposure, based on interface corner critical temperature MCHS model results when the thermal diffusivity is constant, ranged, and variable versus time.

The above-shown data in Figure 20a can be utilized in the assessment of fire-damaged RC, especially for RCC and can be used in design procedures when accounting for fire resistance of HSCC.

For instance, Figure 20b shows that for the same spec-

a

b
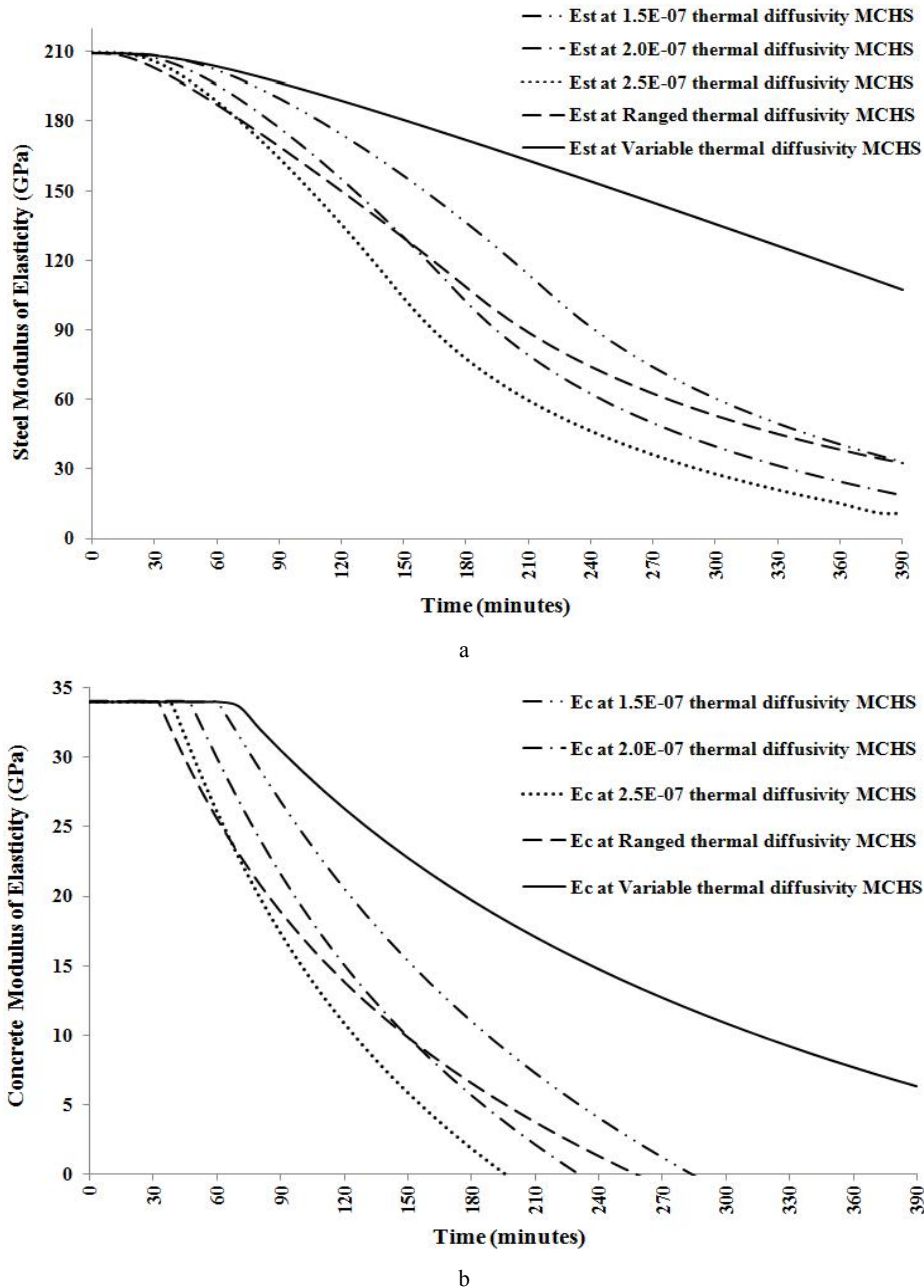
Figure 18. a) Reduction in steel bars modulus of elasticity in MCHS vs. time. b) Reduction in concrete modulus of elasticity in MCHS vs. time.

a

b
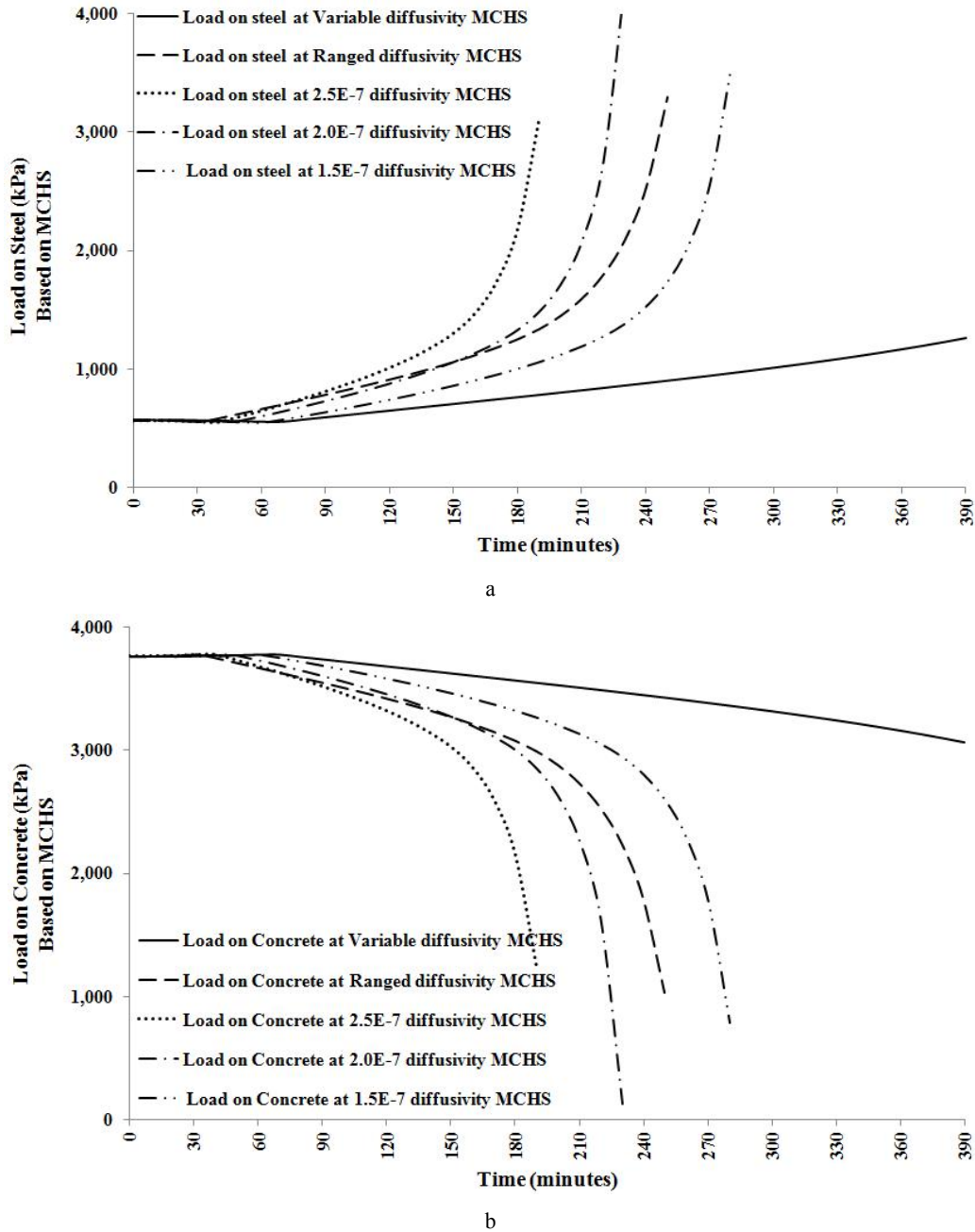
Figure 19. a) Reduction in steel bars modulus of elasticity in MCHS vs. time. b) Reduction in concrete modulus of elasticity in MCHS vs. time.

ification HSCC in the fire exposure scenario the subjected column with 4830 KN load capacity the estimated failure time of a similar column will be about 105 minutes of fire exposure.

Furthermore, if a similar column predicted fire failure load after 30 minutes is required, then it can be determined as shown in Figure 20b which is estimated at around 9470 KN.

Rankine formula RCC Predicted failure Load VS Reinforcement Temperatures

a

b
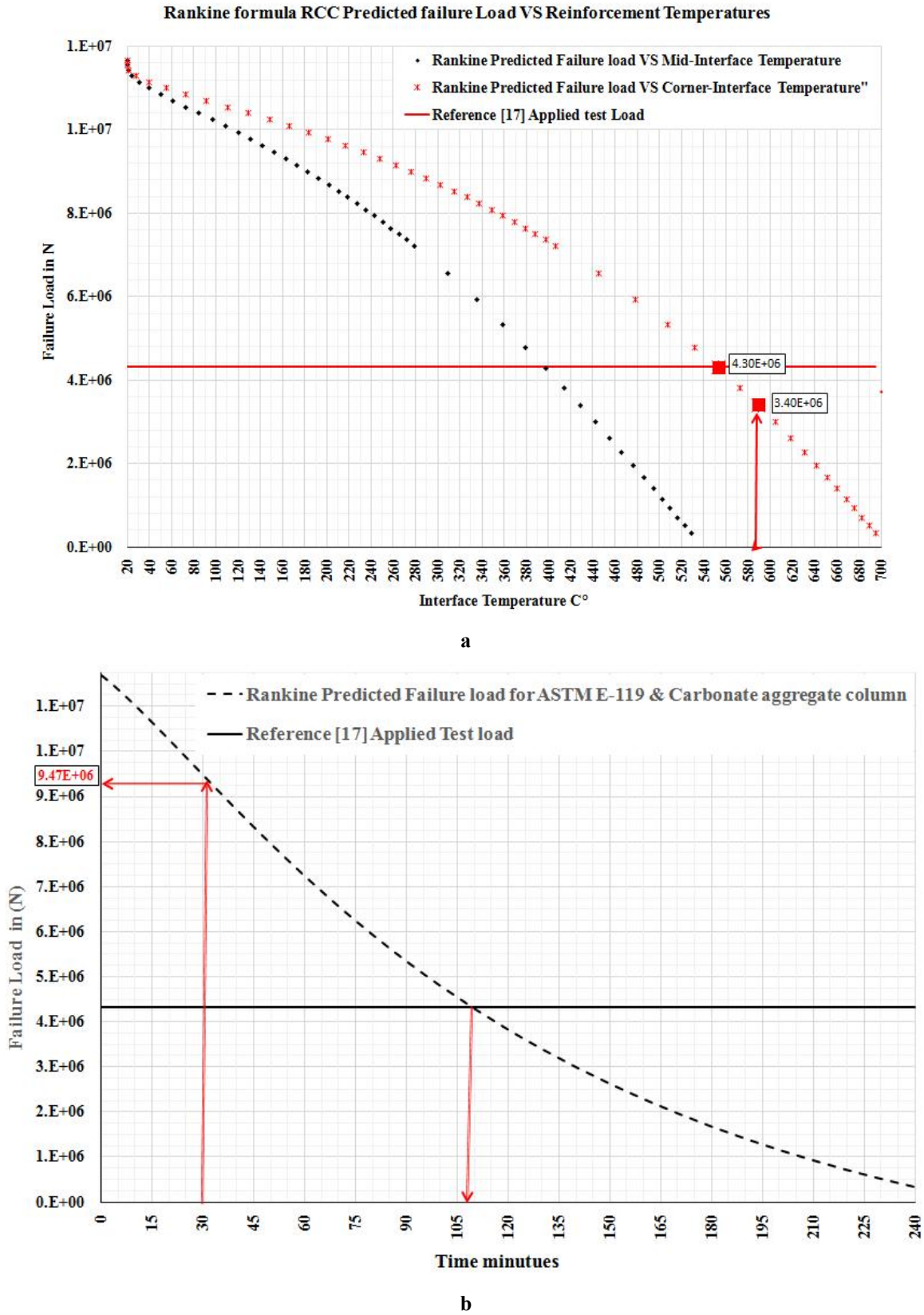
Figure 20. a) HSCC Rankine predicted failure load vs. interface temperatures in MCHS fire exposure. b) HSCC Rankine predicted failure load vs. time in MCHS fire exposure.

4. Conclusions

Based on the experimental and analytical results of this study, the following conclusions can be drawn:

1) The variation in the thermal diffusivity is solid evidence that proves that the thermal and physical properties (K, Cp & p) of the tested material (HSC) have been changed due to fire exposure. Therefore, the nodal temperature is a function of the heating period (time) and the location (depth) of each node. The resulting manipulated and refined correlations of the thermal diffusivity are valid in MCHS for the selected HSCC composed of carbonate aggregate in a hydrocarbon fire.

2) When the interface corner temperature reached 300 °C, the average reduction in steel reinforcing strength was approximately 16.5% and the average reduction in concrete strength was approximately 12%. At 500 °C, the average reduction in steel reinforcing strength was approximately 47.5% and the reduction in concrete strength was approximately 22%–62%. At 600 °C, the average reduction in steel reinforcing strength was approximately 71.11% and the reduction in concrete strength was approximately 40%–85%.

3) At 300 °C, the modulus of elasticity reduced by approximately 27% for concrete and reduced by approximately 11.4% for steel bars. While at 500 °C, the modulus of elasticity was reduced by approximately 64% for concrete and reduced by approximately 32% for steel bars. The effect of elevated temperature on the elastic modulus of elasticity is significant at 600 °C in concrete at 82% and in steel bars at 50%.

4) Two-dimension temperature distribution on HSCC exposed to MCHS in a fire has been predicated with an accuracy that is adequate using a developed simulation model.

5) The results of the thermal simulation branch were compared to previous experimental works and a very good level of agreement was obtained.

6) From the results of the mechanical evaluation branch, performance strength reduction charts were generated which take care of the effect of fire on reinforced concrete.

5. Recommendations

The summarized recommendations and suggestions can be into the following points:

1) The thermal diffusivity of the concrete as well as any other properties input model key parameters should reflect the physical situation. In other words, thermal diffusivity (a) in this study was correlated by the simplest proposed form for MCHS; however in reality it is a sharp function of temperature. This approximation had a pronounced impact on the accuracy of the results. This sensitivity of thermal diffusivity with temperature should be considered for other heating scenarios in any future research in order to observe the effect of this approximation.

2) As this study was based on published experimental work, it recommended that the experimental portion of the research should be performed to confirm this simulation results and another related theoretical study. This can be achieved through the availability of a fire lab to investigate the effect of elevated temperature on any concrete element under a load simulating real-life conditions, not only fixed ends and constant load conditions.

3) Sophisticated, specialized software is commercially-available that simulates the fire condition more comprehensively. However, due to the cost constraint, this software cannot be made available. It is recommended to analyse the effect of elevated temperature on the concrete structure when it is an entire multi-story building as opposed to just a single isolated concrete element. The authors of this study highly recommend the use of such simulation software in order to obtain results for many structural members of the fire-damaged building. This implementation might be of interest to future post-graduate studies as a joint research collaboration between the Departments of Civil Engineering and Mechanical Engineering.

4) Real fire-damaged building theoretical and practical methods of assessment research are highly recommended to be conducted to demonstrate the effect of fire on different types of buildings in Benghazi city after the war. Many of those inside the University of Benghazi.

Conflict of Interest

There is no conflict of interest.

References

[1] Abbasi, A., Hogg, P.J., 2005. A model for predicting the properties of the constitutes of a glass fiber rebar reinforced concrete beam at elevated temperature simulating a fire test. Composites Part B Engineering. 36(5), 384-393.
DOI: https://doi.org/10.1016/j.compositesb.2005.01.005

[2] Ali, F., Nadjai, A., Choi, S., 2010. Numerical and experimental investigation of the behavior of high strength concrete columns in fire. Engineering Structures. 32(5), 1236-1243.
DOI: https://doi.org/10.1016/j.engstruct.2009.12.049

[3] Kang, H.T., Chu, Y.T., 2002. A simple and rational approach for fire resistance prediction of rc columns.

Proceeding of the Second International Workshop "Structures in Fire".

[4] Bratina, S., Cas, B., Saje, M., et al., 2005. Numerical modelling of behavior of reinforced concrete columns in fire and comparison with Eurocode 2. International Journal of Solids and Structures. 42(21-22), 5715-5733.
DOI: https://doi.org/10.1016 /j.ijsolstr. 2005.03.015

[5] Wade, C.A., Cowles, G.S., Potter, R.J., et al., 1997. Concrete blade columns in fire. Concrete 97 Conference, Adelaide, Australia. Conference Proceedings.

[6] Espinos, A., Romero, M.L., Hospitaler, A., 2012. Simple calculation model for evaluating the fire resistance of unreinforced concrete filled tubular columns. Engineering Structures Journal. 42, 231-244.
DOI: https://doi.org/10.1016/j.engstruct.2012.04.022

[7] Ellingwood, B., Shaver, J.R., 1980. Effects of fire on reinforced concrete members. Journal of the Structural Division. 106, 2151-2166.

[8] Wickstrom, U., 1986. A very simple method for estimating temperature in fire exposed concrete structures. London and New York: Elsevier Applied Science Publishers.

[9] Kodur, V.R., Wang, T.C., Cheng, F.P., 2004. Predicting the fire resistance behaviour of high strength concrete columns. Cement & Concrete Composites. 26(2), 141-153.
DOI: https://doi.org/10.1016/S0958-9465(03)00089-1

[10] Federal Emergency Management Agency (FEMA), 2001. Structural Engineering Institute of the American Society of Civil Engineers (SEI/ASCE). World Trade Center Building Performance Study.

[11] Khanna, P.N., Punjab, P.W.D., 1997. Indian Practical Civil Engineering Hand Book.

[12] Kodur, V.R., Kacianauskas, R., Raftoyiannis, I.G., et al., 2014. Properties of concrete at elevated temperatures. International Scholarly Research Notices.
DOI: http://dx.doi.org/10.1155/2014/468510

[13] Dwaikat, M., Kodur, V.R., 2009. Hydrothermal model for predicting fire-induced spalling in concrete structural systems. Fire Safety Journal. 44(3), 425-434.
DOI: https://doi.org/10.1016/j.firesaf.2008.09.001

[14] Sethuraman, V.S., Suguna, K., 2016. Computation of modulus of elasticity of high strength concrete using silica fume. Asian Journal of Applied Sciences. 4(1), 54-62. Available from: www.ajouronline.com.

[15] Kodur, V.R., Dwaikat, M., Raut, N., 2009. Macroscopic fe model for tracing the fire responses of reinforced concrete structures. Engineering Structures. 31(10), 2368-2379.
DOI: https://doi.org/10.1016/j.engstruct.2009.05.018

[16] Kodur, V.R., Ahmed, A., Dwaikat, M., 2009. Modeling the fire performance of frp-strengthened reinforced concrete beams. Composites & Polycon. The American Composites Manufacturers Association (ACMA)'s annual convention and exhibition.

[17] Kodur, V.R., McGrath, R., Leroux, P., et al., 2005. Experimental studies for evaluating the fire endurance of hsc columns. National Research Council Canada.
DOI: https://doi.org/10.4224/20378032

[18] Yaqub, M., Bukhari, I.A., Ghani, U., 2012. Assessment of residual strength based on estimated temperature of post-heated rc columns. Journal of Engineering and Technology. 32(1), 55-70.

[19] Blagojevic, M.D., Pesic, D.J., 2011. A new curve for temperature-time relationship in compartment fire. Thermal Science. 15(2), 339-352.
DOI: https://doi.org/10.2298/TSCI100927021B

[20] Kumar, P., 2004. Rectangular rc columns subjected to fire load. Journal of the Institution of Engineers Civil Engineering Division Board. 85, 186-192.

[21] Hsu, J.H., Lin, Ch.Sh., Huang, Ch.B., 2005. Modeling the effective elastic modulus of rc beams exposed to fire. Journal of Marine Science and Technology. 14(2), 102-108.
DOI: https://doi.org/10.51400/2709-6998.2063

[22] Gopinathan, K.K., 1990. Solar radiation on inclined surfaces. Solar Energy. 45(I), 19-25.
DOI: https://doi.org/10.1016/0038-092X(90)90062-H

[23] Nash, W.A., 1984. Strength of materials. Civil Engineering Machaustus University, McGraw Hill, Dar Alraed Al-Arabie, Beirut—Lebanon, P.O. Box 6585, Telex L.E 43499.